

A Feed-forward Neural Network Algorithm to Detect Thermal Lesions Induced by High Intensity Focused Ultrasound in Tissue

Parisa Rangraz, Hamid Behnam¹, Naser Shakhssalim², Jahan Tavakkoli³

Department of Biomedical Engineering, Science and Research Branch, Islamic Azad University, ¹Iran University of Science and Technology/School of Electrical Engineering, ²Shahid Labbafinejad Medical center, Urology and Nephrology Research Center (UNRC), Shahid Beheshti University of Medical Sciences, Tehran, Iran, ³Department of Physics, Ryerson University, Toronto, Ontario, Canada

Submission: 23-07-2012

Accepted: 09-09-2012

ABSTRACT

Non-invasive ultrasound surgeries such as high intensity focused ultrasound have been developed to treat tumors or to stop bleeding. In this technique, incorporation of a suitable imaging modality to monitor and control the treatments is essential so several imaging methods such as X-ray, Magnetic resonance imaging and ultrasound imaging have been proposed to monitor the induced thermal lesions. Currently, the only ultrasound imaging technique that is clinically used for monitoring this treatment is standard pulse-echo B-mode ultrasound imaging. This paper describes a novel method for detecting high intensity focused ultrasound-induced thermal lesions using a feed forward neural-network. This study was carried on *in vitro* animal tissue samples. Backscattered radio frequency signals were acquired in real-time during treatment in order to detect induced thermal lesions. Changes in various tissue properties including tissue's attenuation coefficient, integrated backscatter, scaling parameter of Nakagami distribution, frequency dependent scatterer amplitudes and tissue vibration derived from the backscattered radio frequency data acquired 10 minutes after treatment regarding to before treatment were used in this study. These estimated parameters were used as features of the neural network. Estimated parameters of two sample tissues including two thermal lesions and their segmented B-mode images were used along with the pathological results as training data for the neural network. The results of the study shows that the trained feed forward neural network could effectively detect thermal lesions *in vitro*. Comparing the estimated size of the thermal lesion (9.6 mm × 8.5 mm) using neural network with the actual size of that from physical examination (10.1 mm × 9 mm) shows that we could detect high intensity focused ultrasound thermal lesions with the difference of 0.5 mm × 0.5 mm.

Key words: Feed forward neural network, high intensity focused ultrasound lesion detection, Nakagami distribution, tissue mechanical and acoustical parameters

INTRODUCTION

Proper guidance and monitoring of high intensity focused ultrasound (HIFU) treatment is essential for its wide spread clinical acceptance. Several imaging techniques have been used towards monitoring and control of HIFU treatments.^[1-3] Besides the importance of imaging pre-and during treatment, post-treatment imaging to map the treated region for follow-up and/or continued therapy must also be considered. The most common non-ultrasound-based HIFU treatment monitoring and control methods consist of: X-ray and magnetic resonance imaging (MRI).^[3] The feasibility of using MRI to detect HIFU-induced tissue necrosis has extensively been studied.^[4-6] Moreover, a number of studies have been carried out proposing ultrasound imaging for this purpose. Conventional B-mode ultrasound imaging does not have enough accuracy and specificity for reliable

detection of the HIFU-induced thermal lesions.^[7-13] Transient characteristics of tissue's integrated backscatter (IBS), attenuation coefficient and bubble activities as time traces before, during and after HIFU treatment have been investigated to this end.^[11,12] A dramatic increase in both attenuation and IBS values were observed during the HIFU therapy which may be attributed to significant enhancement of bubbles activity in the focal region (cavitation and/or boiling bubbles), and accompanying tissue damage.^[11,12]

Recent researches have shown the potential of using radiation force impulses to monitor displacement changes that may be related to the formation of the HIFU thermal lesion. It has been suggested that as the thermal lesion forms a reduction in displacement should occur. More recent publications have reported initial increases in the displacements prior to stiffening.^[13-17] It has been proposed an ultrasonic Nakagami

Address for correspondence:

Dr. Parisa Rangraz, Department of Biomedical Engineering, Science and Research Branch, Islamic Azad University, Tehran, Iran.
E-mail: p.rangraz@srbiau.ac.ir

imaging technique to monitor HIFU thermal ablation in real time and it has been demonstrated that Nakagami could detect the HIFU-induced thermal lesion, which was difficult to be located in conventional B-mode images because of no appearances of bubbles and Nakagami images showed higher contrast in the cases with apparent bubble formation.^[18] On the other hand, several types of neural network algorithms have been used for segmenting ultrasound images. These include Kohonen network, incremental self-organized map (ISOM), restricted coulomb energy networks, and multi-layer perceptron (MLP) network.^[19-21]

The aim of any classification method is to classify objects into two or more groups based on object attributes.^[22] The work presented in this paper describes an automatic method for detecting HIFU-induced thermal lesions using a feed forward neural network. We estimated some acoustical and mechanical and statistical parameters of tissue such as attenuation coefficient, IBS, scaling parameter of Nakagami distribution, frequency dependent scatterer amplitudes, and tissue vibration based on real-time acquired radio frequency (RF) data and used them as features to run a multi-layer perceptron (MLP) neural network. The MLP is a multi-layer feed forward neural network which is a supervised classifier. It contains one or more hidden layers for which their neuron's function is to arbitrate between the input and the output layers.^[22,23] RF data acquired from two samples of tissues were used in this study. The first sample used to estimate the features for training of the neural network, and the second sample of tissue was used as the test data for the algorithm. We tried to find the best features to run the neural network so the implemented neural network was run using various combinations of the mentioned parameters to investigate which output of the neural network is more close to actual target. From this study, it was concluded that the best result is obtained when all of the mentioned parameters are used as input features to the neural network.

MATERIALS AND METHODS

Image-guided HIFU System

A1-MHz, F#0.8, and 125 mm aperture diameter transducer (Imasonic S.A., Besançon, France) were used in this study to deliver the therapeutic ultrasound energy. Derived from simulations and verified by measurements, the full width at half maximum (FWHM) lateral and axial dimensions of the HIFU beam focal spot in water were 1.7 mm and 6.8 mm, respectively. A Sonix RP® clinical ultrasound scanner (Ultrasonix Medical Corp., Richmond, BC, Canada) was used to acquire RF echo data and to monitor HIFU thermal lesion formation and growth in real time pre-, during and post-exposure via its endocavity 4-MHz convex array probe which was coaxially mounted in the centre of the therapy transducer. Figure 1 shows the confocal arrangement

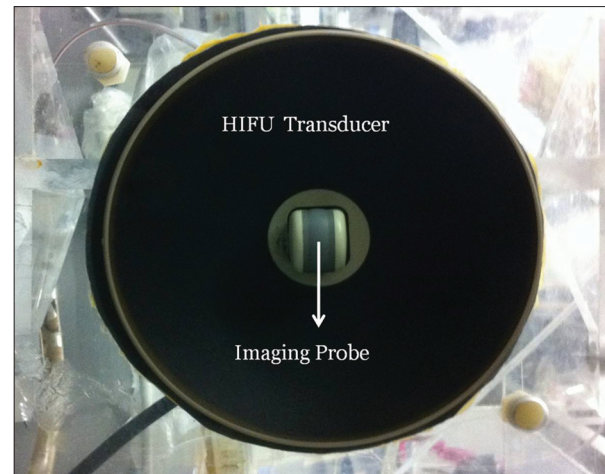


Figure 1: Confocal arrangement of the imaging probe with the HIFU transducer

of the imaging probe and the HIFU transducer. An AFG3101 arbitrary function generator (Tektronix Inc., Beaverton, OR) provided the input electrical bursts to an AG1012 RF power amplifier (T and C Power Conversions Inc., Rochester, NY) which in turn derived the HIFU transducer. A typical HIFU exposure was 40 s of 45-W acoustic power delivered with a 77% duty cycle. The HIFU exposures induced thermal lesions in the pork muscle tissue *in vitro*.

Tissue Parameters Estimation

Estimation of several mechanical and acoustical parameters of tissue through processing of the backscattered ultrasound RF data has been studied as part of this research and is briefly described below.

Attenuation coefficient

Many methods have been studied to estimate attenuation coefficient which are reviewed in.^[24] The transient characteristics of tissue attenuation coefficient were investigated before, during and after HIFU treatment.^[25] A common spectral difference attenuation estimation method to measure changing in attenuation coefficient during HIFU exposure, known as the multi-narrow-band (MNB) method used by.^[11] The different segments according to the depth were windowed along an RF A-line from one backscattered RF data frame from the tissue. Under the assumption that the backscatter coefficient was the same in each small segment, the power spectra of the RF data backscattered from the front and back of a segment can be given by Eq. (1) 11:

$$S_b(\Delta d) = S_f(\Delta d) | H(\Delta d) |^2 \quad (1)$$

Where $S_f(\Delta d)$ and $S_b(\Delta d)$ are the power spectra of the front and back of a segment with the (Δd) thickness. $H(\Delta d)$ is the transfer function of this segment. Figure 2 is a graphical representation of the two spectra, $S_f(\Delta d)$ and $S_b(\Delta d)$ for a typical representative RF data 24.

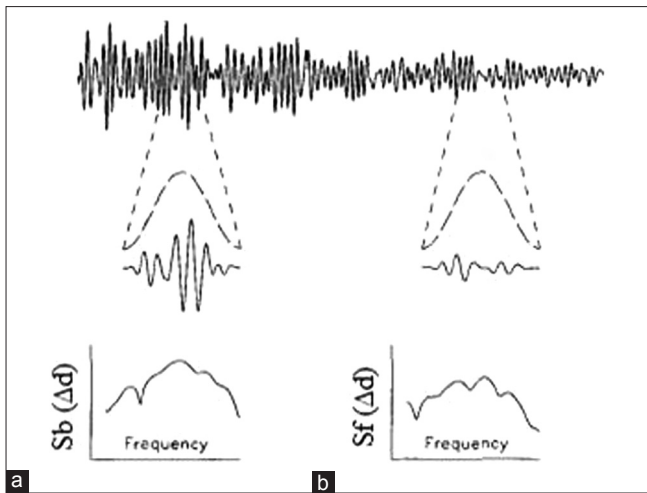


Figure 2: Back (a) and front (b) of a segment windowed from a hypothetical RF A-line and Fourier transformed to yield the corresponding $S_b(\Delta d)$ and $S_f(\Delta d)$ ^[24]

By considering the effects of attenuation, the $H(\Delta d)$ was approximated as:

$$|H(\Delta d)| = e^{-2\Delta d \Delta \alpha(\Delta d)} \quad (2)$$

The tissue attenuation coefficient was estimated by subtracting the log power spectra of the back segment from the log power spectra of the front segment. Spatial averaging in the segment was then used to reduce the variance because of noisy statistical ensemble of scatterers echo signal.^[11]

$$\Delta \alpha(\Delta d) = \ln \frac{S_f(\Delta d)}{S_b(\Delta d)} / (4 \Delta d) \quad (3)$$

$$A = \text{mean} [\Delta \alpha(\Delta d)]$$

In this study, the pre-, during- and post-HIFU backscattered RF data were registered with the assumption that the position of the tissue sample is constant. The log power spectra of the segments of the pre-data were considered as the references or the back segment in Eq. (3). The log power spectra of the segments of the post-data in the same position were considered as the front segment in Eq. (3) and compared with the references to estimate the change in the tissue attenuation coefficient using the Eq. (3).

Integrated backscatter

Ultrasonic integrated backscatter has shown the potential to provide the information of micro-structure in tissue^[26] which may alter when tissue is affected by HIFU exposure. The IBS can be determined by:^[11,12,27]

$$\text{IBS} = \frac{1}{2\Delta f} \int_{f_0-\Delta f}^{f_0+\Delta f} \ln \frac{P(f, T_2)}{P(f, T_1)} df \quad (4)$$

Where f_0 is the center frequency of the transmitted pulse, Δf is half of the usable bandwidth, $P(f, T_2)$ and $P(f, T_1)$ are the

power spectra of the signals backscattered from the tissue. T_1 and T_2 are two different frame times.^[12] In this study, the IBS was estimated with a similar technique which was used for the attenuation estimation. The signal segments acquired post-HIFU were compared to those related to pre-HIFU in the same position.

Frequency Dependent Scatterer Amplitudes

Frequency dependence of backscattering to characterize tissue has been studied by various groups.^[28-30] As frequency dependence of the backscatter coefficient is related to the tissue microstructure, it is an important parameter for ultrasonic tissue characterization. The frequency dependence of the backscatter coefficient depends primarily on the size distribution of the scatterers.^[28,29]

In this study we estimated changes in scatterers' size due to HIFU exposure. To this end, we transmitted signals in two different frequencies of 2 and 4 MHz. To this end, we transmitted signals in two different frequencies of 2 and 4 MHz. Then using the following equation we found the difference between the pressure amplitudes of second and main harmonic of backscattered signals:

$$A = \frac{d}{dz} [P_{L1}(f_0, z) - P_{L2}(2f_0, z)] \quad (5)$$

Where P_{L1} and P_{L2} are the amplitudes of the second harmonic of backscattered echo signals with transmitted central frequency of two MHz and the amplitudes of the main harmonic of backscattered echo signals with transmitted central frequency of four MHz, respectively, and z represents the depth.

Nakagami parameter

The Nakagami statistical distribution has recently received considerable attention toward processing of ultrasound RF data.^[31,32] The corresponding Nakagami parameter estimated from the backscattered echo signals can be used to identify various backscattering distributions in medical ultrasound, thereby providing the ability to characterize biological tissues.^[33,34]

The Nakagami image is based on the statistical distribution of the backscattered signals, hence provides information about the arrangements of scatterers in a scattering medium such as tissue.^[32,34] It has been shown that the probability density function (pdf) of the ultrasonic backscattered envelope R under the Nakagami statistical model is given by:^[32,34,35]

$$f(r) = \frac{2m^m r^{2m-1}}{\Gamma(m)\Omega^m} \exp\left(-\frac{m}{\Omega} r^2\right) U(r) \quad (6)$$

where $\Gamma(\cdot)$ and $U(\cdot)$ are the gamma function and the unit step

function, respectively. The symbol r represents possible values for the random variable R of the backscattered envelopes. Let $E(\cdot)$ denote the statistical mean. Both the Scaling and Nakagami parameters associated with the Nakagami distribution can be calculated as follows:^[32,34,35]

$$\Omega = E(R^2) \tag{7}$$

$$m = \frac{[E(R^2)]^2}{E[R^2 - E(R^2)]^2} \tag{8}$$

The Nakagami parameter as a function of scatterer concentration and the Scaling parameter signifying the average energy in the backscattered echo were both calculated using backscattered signals. In this study, the Scaling parameter was estimated and used as another feature for the neural network.

Tissue vibration

The Hilbert transform of echo signals were calculated to determine tissue vibrations due to ultrasound radiation force. At first we calculated the correlation between amplitude of the Hilbert transform of RF lines of two subsequent frames then the differences between the phases of Hilbert transforms of the signal of the first frame and shifted signals of the second frame were calculated. The tissue vibration in tissue sample because of radiation force was estimated by:

$$x = \frac{\phi \times \lambda}{2\pi} \tag{9}$$

where x is the tissue vibration, ϕ is phase change and λ represents the wave length.^[36] It was expected that the tissue vibrations values calculated using the above equation would be different between the part of tissue where the thermal lesion was induced and the surrounding normal tissue.

Feed forward neural networks

There are two groups of neural network classifiers: Supervised and unsupervised. Supervised classifiers use known output data whereas unsupervised methods rely on input data to classify.^[19,22] Layered feed forward neural network is the most common type of neural network used in engineering applications.^[19,22] Multi-layer perceptron (MLP) contains a number of neurons, where the function of each neuron is to combine input data using weighted sum operation and pass the resulting sum through output neuron. The number of layers and neurons in each layer depend on the nature of the problem.^[22,37]

In this method, the output of neuron i , driven by N inputs x_j , each with weight ω_{ij} , is given by:

$$s_i = g(\sum_{j=0}^N \omega_{ij}x_j) \tag{10}$$

where $g()$ is the sigmoid function and is given by:^[19-21]

$$g(x) = \frac{1}{1 + e^{-x}} \tag{11}$$

In our study, a feed forward neural network was used including five features as inputs, one hidden layer with three neurons and one neuron as the output layer with the sigmoid function. Therefore, it is called a 5-3-1 network. Figure 3 shows the schematic view of our neural network, including input, hidden and output layers. As the number of features is five and there are three neurons in hidden layer the number of weights are 18 so the number of samples must be more than 10×18 so we have enough data to run the neural network.

RESULTS

Figure 4 shows the B-mode image from the Sonix RP scanner. Two pieces of Porcine muscle tissue were prepared

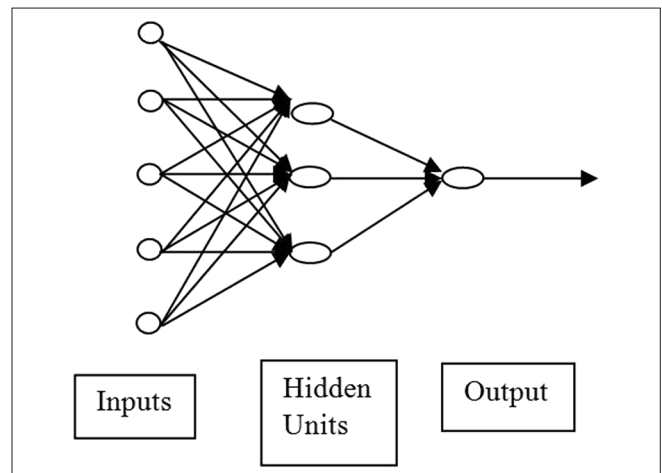


Figure 3: Schematic of the three-layer feed forward neural network which is used in this study

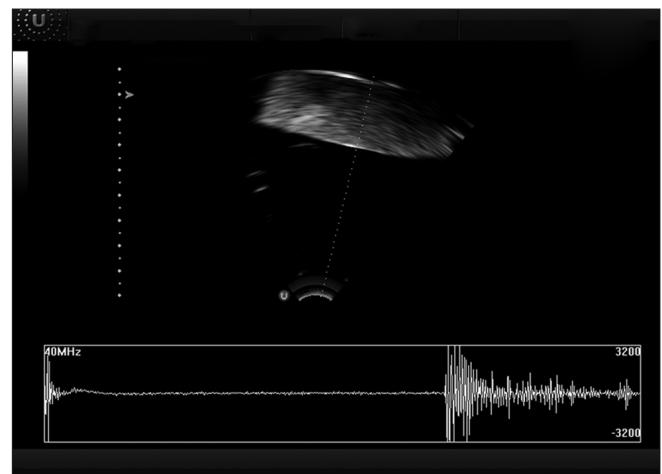


Figure 4: B-mode image from Sonix RP monitor related to pre-HIFU experiment

and used in this study. Different numbers of HIFU lesions were induced in each of them. For each lesion, the pre-HIFU RF data and B-mode image were acquired. HIFU exposure was on for 40 seconds to induce a thermal lesion. The post-HIFU RF data and B-mode image were acquired at 10 minutes after the HIFU turned off. The region of interest of B-mode image of this frame was separated to estimate the parameters of interest. Figure 5 shows the selected region of interest of reproduced B-mode images of one of the lesions (Tissue #6: Lesion#4) used as the train data corresponding to pre-, during- and post- HIFU.

A moving hamming window was used to segment each RF data line in such that it divides into a series of segments of length 0.9 mm (60 sample points), assuming ultrasound speed of 1540 m/s in tissue. The tissue was put in a holder, so the position of it was fixed during acquiring pre and post-data for each lesion. This made it possible to compare two registered images for a point by point analysis.

The lateral distance between two neighbouring lesions was approximately 1cm. From lesions created, two lesions (Tissue#6: Lesions#4,6) were used as the train data and the other two as the test data (Tissue#2: Lesions#2,5). In order to choose the lesions to be used as train data, at first we estimated the parameters of Tissue#6: Lesions#4,5,6. We trained the neural network using different mixture of two lesions among these three lesions. Test error of neural network using Lesion#4,6 as train data was 0.0018 which was less than test error of Lesion#4,5 as train data which was 0.0093, and test error of neural network related to Lesion#5,6 as train data which was 0.011. So we used Lesion#4,6 as train data. In the following, first the images of estimated parameters of the train data set related to Tissue#6: Lesion#4 and then the results of test data set related to Tissue#2: Lesion#2 will be presented. Because of large number of images estimated for four lesions, we only present the results of one of the train and one of the test data set to be able to tracking changes of parameters and also compare the result of detecting lesions with and

without the neural network. At the end, images produced from the results of neural network will be presented.

Using the corresponding equations and implemented algorithms, all parameters subject to this study were calculated and imaged. Figure 6 shows the corresponding images of post values of estimated attenuation coefficient, IBS, scaling parameter of the Nakagami distribution, frequency dependent scatterer amplitudes and tissue vibration divided by the corresponding pre values. Regarding to colorbar of the images, it is seen that Attenuation coefficient, IBS, scaling parameter of the Nakagami distribution, and frequency dependent scatterer amplitudes in the HIFU lesion site were increased whereas the tissue vibration of the lesion was decreased.

Besides estimated parameters of Tissue#6: Lesion#4, parameters of Tissue#6: Lesion#6 were estimated and used as train data for neural network. After using these data to train the network two other lesions (Tissue#2: Lesions#2,5) were used for test. Figure 7 shows selected site of reproduced B-mode images of one of the lesions (Tissue#2: Lesion#2) used as test data for pre-, during-and post-HIFU. Figure 8 shows the corresponding images of attenuation coefficient, IBS, scaling parameter of the Nakagami distribution, frequency dependent scatterer amplitudes, and tissue vibration. As in the previous lesion, the attenuation coefficient, IBS, scaling parameter and frequency dependent scatterer amplitudes in the lesion site were increased whereas the tissue vibration of lesion was decreased.

This information (related to Tissue#2: Lesion#2) besides estimated parameters of Tissue#2: Lesion#5 were used as test data. The values of the neural network for a pixel of interest are either one or zero for being coagulated or not being coagulated, respectively.

For training the network we needed to distinguish a lesion from the surrounding normal tissue, so the post-HIFU B-mode images along with physical examination of tissue cut

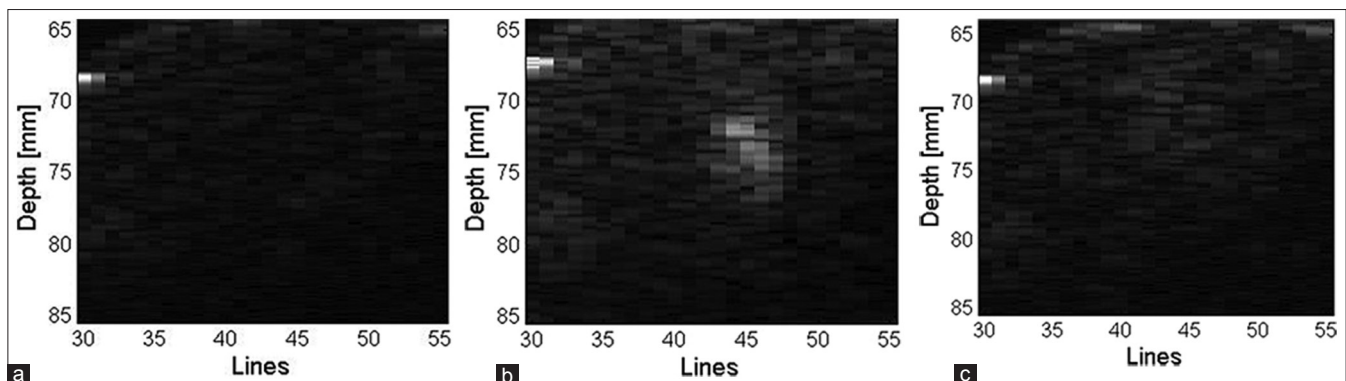


Figure 5: Selected region of interest of reproduced B-mode images for pre-, during- and post-HIFU related to Tissue#6:Lesion#4. (a) pre- (b) during- and (c) post- images

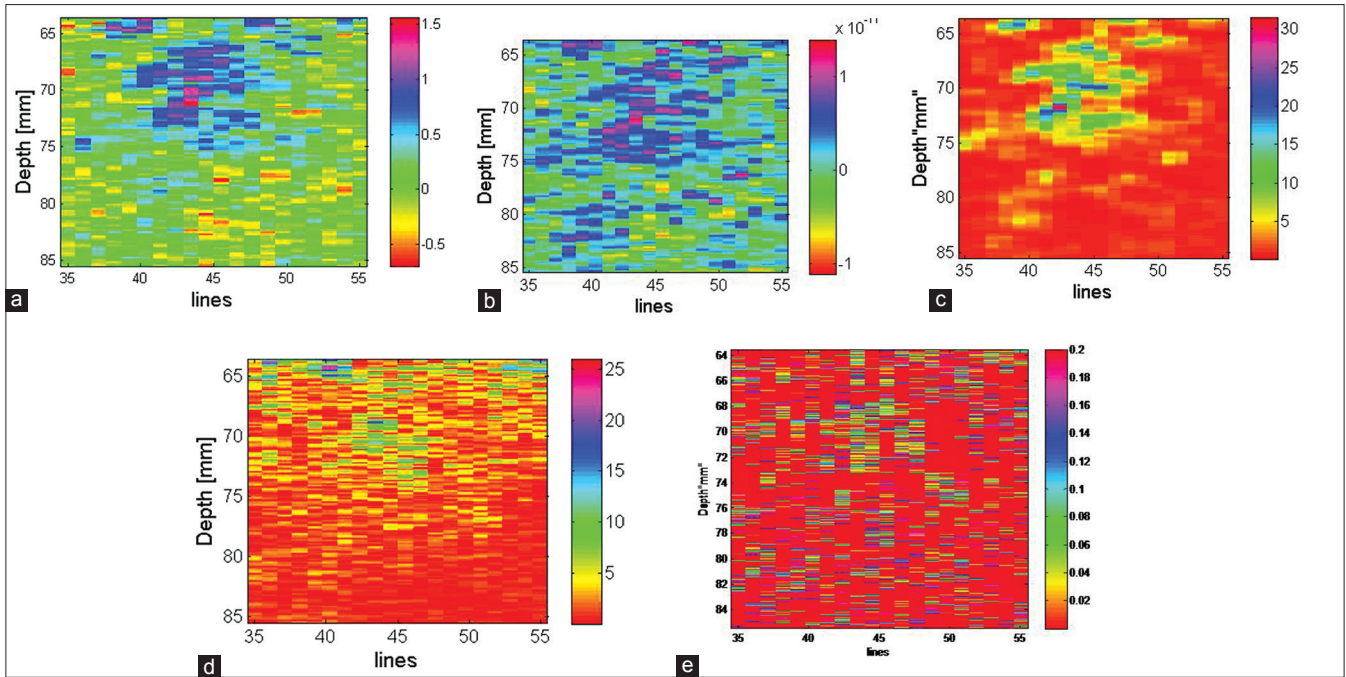


Figure 6: Tissue#6: Lesion#4 (a) Attenuation coefficient, (b) IBS, (c) Scaling parameter of Nakagami distribution, (d) frequency dependent scatterer amplitudes, and (e) tissue vibration images

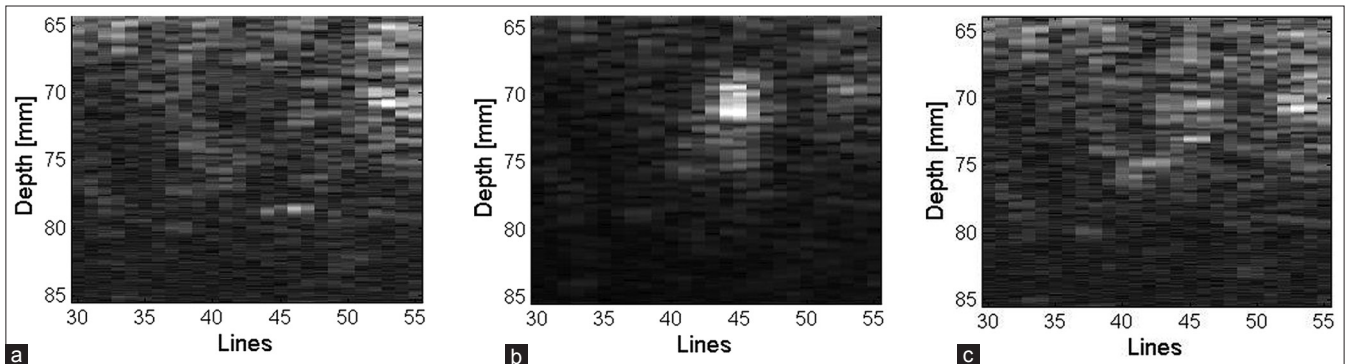


Figure 7: Selected region of interest of reproduced B-mode images regarding to pre-, during- and post-HIFU related to Tissue#2: Lesion#2. (a) pre- (b) during- (c) post- images

and the B-mode image registered during HIFU were used to be able to distinguish a lesion site from the normal tissue. For training and testing neural network we used the pixels in the regions of the tissue where the existence of the normal or coagulated tissues was certain. To this end, we first located the centre of the lesion using B-mode images acquired during HIFU and then using the lesion size measured after tissue cut we estimated which pixels were coagulated. These pixels in the centre of the lesion corresponding to the coagulated tissue were then chosen to train and test the MLP neural network algorithm. The training error (mean square error between the network output and the actual target of train data^[37]) of this network was calculated as 9.14×10^{-12} and the test error (mean square error between the network output and the actual target of test data) was calculated as 0.0018.

The trained neural network was used to segment all the sites

of interest of data related to tissue samples. We neglected the areas detected by the neural network algorithm as lesion if it's lateral dimension was less than 1.7 mm, We used this value as the FWHM Lateral dimension of HIFU beam focal spot in water was 1.7mm and assumed that as normal tissue. Figure 9 shows the result of neural network for detecting Tissue#2: Lesion#2. Comparing the size of detected lesion (9.6 mm \times 8.5 mm) with the actual size of the lesion from physical examination (10.1 mm \times 9 mm) shows that we could detect a lesion with the difference of 0.5 mm \times 0.5 mm.

Table 1 compares the detected size of Lesion#2 of Tissue#2 (Depth \times Length) using the mentioned parameters based on each imaged parameter and also using the neural network algorithm developed in this study. It is seen that the neural network can effectively detect the actual lesion size which is 10.1 mm \times 9 mm.

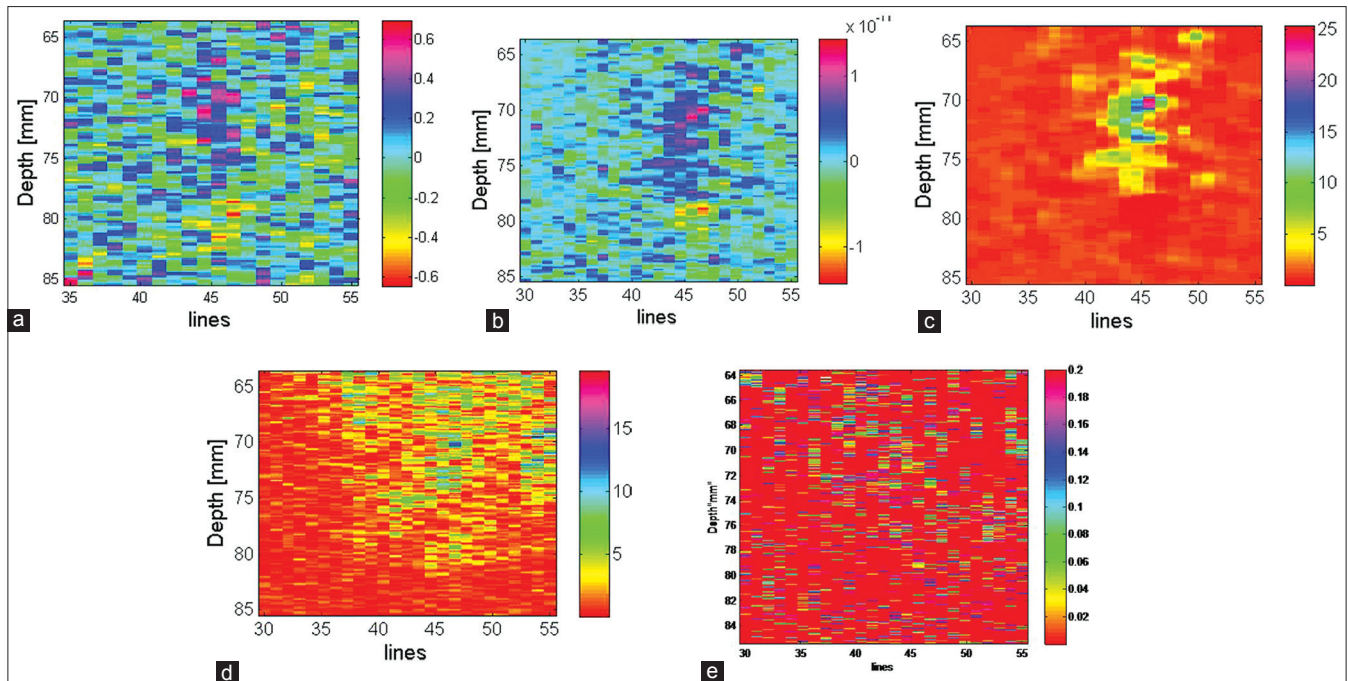


Figure 8: Tissue#2:Lesion#2 (a) attenuation coefficient, (b) IBS, (c) scaling parameter of Nakagami distribution, (d) frequency dependent scatterer amplitudes, and (e) tissue vibration images

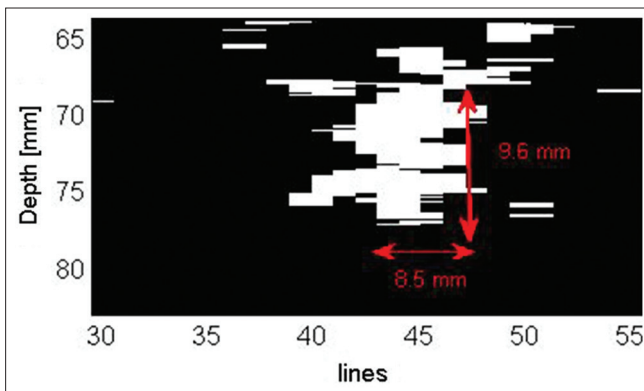


Figure 9: Segmentation of normal and coagulated tissue by 5-3-1 neural network

Table 1: Detected size of high intensity focused ultrasound induced-Lesion#2 (Tissue#2) using different methods

Parameters	Measured lesion size (mm×mm)
Attenuation	6.8×5.1
IBS	10.1×6.8
Scaling parameter of Nakagami distribution	8×8.6
Parameter of scatterers' size changes	6×6.8
Vibration	5.2×5
MLP neural network	9.6×8.5

IBS – Integrated backscatter; MLP – Multi-layer perceptron

The neural network was run using various combinations of the mentioned parameters to find out which combination causes in best result (output of the neural network is more close to actual target) So six scenarios were studied, in each scenario we neglected one of the parameters then we found the

sensitivity of the output of neural network to absence of that parameter. The difference of actual area (Depth × Length) of lesion with the estimated area using each scenario divided by the actual area used as indicator of the sensitivity also we substituted the actual area with the estimated area using all parameters combination to determine proportional accuracy. The best parameters combination is selected based on the determined sensitivities. Table 2 compares the determined sensitivities for detecting Lesion#2 of Tissue#2. This table includes the information of all scenarios' results and it shows that the best result is obtained when all of the mentioned parameters are used as input features to the neural network. Estimated sensitivities using actual size illustrates that the estimated area using all parameters without Scaling parameter of Nakagami distribution can result in highest error which means this parameter is so effective in lesion detection. Comparing the estimated sensitivities of other scenario shows other parameters help in more accurate detecting of lesion. In the last column of table, each scenario has been compared with the estimation using all parameters and their sensitivities have been compared with the best scenario. It shows that Scaling parameter of Nakagami distribution causes in highest error in estimating lesion size and the vibration is less effective in the neural network.

Physical Examination of Tissue

After acquiring all RF data, the tissues were cut into slices and photographed for gross pathology examinations. Figure 10 shows the tissue#6 in which estimated parameters of lesions#4, 6 were used as the neural network train data. Figure 11 shows the tissue#2 in which

Table 2: The determined sensitivity of the output of neural network for detecting Lesion#2 of Tissue#2 using different combination of features

Scenario description	Depth (mm)	Length (mm)	Area	Deviation from actual size (%)	Deviation from all parameter included (%)
Actual size	10.1	9	90.9	0.0	-
S1 All parameters included	9.6	8.5	81.6	-10.2	0.0
S2 All parameters without attenuation	9.2	8.5	78.2	-14.0	-4.2
S3 All parameters without scatters' size changes	9.2	8.3	76.36	-16.0	-6.4
S4 All parameters without vibration	9.4	8.5	79.9	-12.1	-2.1
S5 All parameters without IBS	8.7	8.3	72.21	-20.6	-11.5
S6 All parameters without scaling parameter of Nakagami distribution	5	6.8	34	-62.6	-58.3

IBS – Integrated backscatter

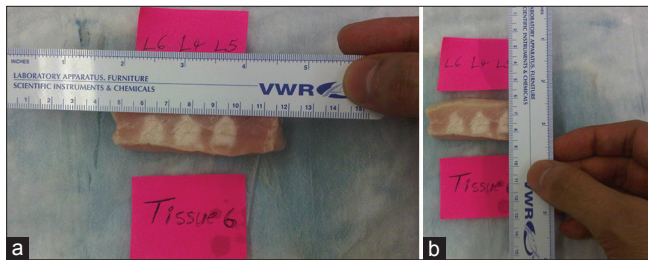


Figure 10: Tissue cut and folded open, showing HIFU lesions in its middle part (a) measuring length of the lesion. (b) measuring depth of the lesion

estimated parameters of lesions#2, 5 were used as the test data.

DISCUSSIONS

It is observed in this study that after the HIFU exposure, attenuation coefficient and IBS values increase in the treated area, as mentioned in previous studies.^[11,12] Studied the dynamic changes of attenuation coefficient and IBS for different acoustic powers. For their presented phantom, it was shown that one night after treatment the attenuation coefficient was almost thrice that before and the increase in IBS was about 5% also they placed the treated bovine livers in a cold room overnight at a temperature of 4 °C and after that the estimated IBS and attenuation coefficient further decreased comparing to during time of treatment but were still higher than before HIFU treatment. In our study, the average of the estimated attenuation coefficient in lesion site increased about 0.7 dB/cm comparing to before HIFU treatment. Also the averaged estimated differential IBS in the lesion site was increased about 5×10^{-11} times comparing to before HIFU treatment. The difference in our work comparing with the previously published works is in the choosing of reference segments for calculating the attenuation coefficient and IBS. Here, the log power spectra of the segments of the pre-data were considered as the references. After HIFU exposure, the backscattered signal usually yields lower SNR because of increased attenuation in the focal area that attenuates the signal from the post focal

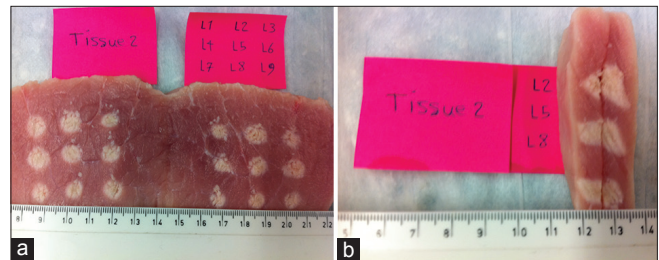


Figure 11: Tissue cut and folded open, showing HIFU lesions in its middle part. (a) Tissue cut and folded from middle to measure length of the lesion. (b) Tissue folded close and cut vertically to measure depth of the lesion

region. As suggested in,^[12] the tissue albumen coagulation causes an increase in attenuation due to structural effect. Figures 6c and 8c showed that Scaling parameter of Nakagami distribution increases in the site of HIFU lesion too. This parameter is representation of the average energy in the backscattered signal and because of structural effect of the HIFU lesion and increase in attenuation, it is expected that the average backscattered energy from the lesion site would be higher. It has been shown that tissue stiffness decreases initially during heating and starts to increase if heated above a certain temperature threshold.^[15,16] Different attempts have been made to estimate stiffness-related parameters within tissues, such as strain measurements, tissue displacement under a localized force, response to vibration and ultrasound-stimulated acoustic emission (USAE) of tissues.^[15] In our work, as it is shown in Figures 6e and 8e, the tissue vibration in the lesion site is decreased after HIFU treatment. Here we implemented a simple method to estimate the tissue vibration based on only the backscattered RF data that was acquired using an imaging probe without any higher intensity beam for pushing tissue samples. As Figures 6d and 8d show the frequency dependent scatterer amplitudes increases after the HIFU treatment. This could be attributed to the fact that the size of scatterers change after HIFU treatment and it can be used as a parameter to detect HIFU lesions.

While the neural network training process creates a nonlinear mapping between input and output, the choice

of input data for network is critical, along with the choice of features. The processing method applied here is based on the measurement of experimental tissue cut and during-HIFU B-mode images to find if any pixel is coagulated or not. One challenging point in doing accurate lesion size measurements is due to the fact that when we cut tissue we do not exactly know the B-mode image and acquired RF lines belong to which slice in order to exactly compare the real sizes with the estimated ones. But using physical examination of the tissue cut besides the B-mode images acquired during HIFU can help us to have a good estimation.

CONCLUSIONS

A non-invasive ultrasound-based technique to detect the thermal lesions induced by HIFU exposures was developed based on characteristics of mechanical, acoustical and statistical properties of pork muscle tissue *in vitro*. The tissue parameters including attenuation coefficient, IBS, frequency dependent scatterer amplitudes, tissue vibration, and scaling parameter of Nakagami distribution were estimated and imaged based on ultrasound backscattered RF data which was acquired 10 minutes after HIFU when the reference ones acquired before HIFU exposure. Selected samples of these data were used for training of and testing the neural network. This paper presents a simple 5-3-1 feed forward neural network that has been trained to segment and detect HIFU lesion in registered data. Each individual tissue parameter might be able to detect a lesion within its own limitations, but using all of them simultaneously can make significant improvement in the detection of true size of lesion. If in a situation one of the acoustical, mechanical or statistical parameter could not detect a lesion, using all of them can significantly enhance the lesion detect-ability. As a future step in this work, we plan to use this neural network to monitor HIFU lesion initiation and growth in real time. Moreover, the proposed technique is not limited to HIFU therapy and has a potential to be applied to other thermal therapies such as RF or microwave. It is concluded that still a great deal of additional training is needed before this technique can be applied in clinical settings.

ACKNOWLEDGMENTS

We would like to thank Mr. Pooya SobheBidari and Mr. Siavash Rahimian from Dept. of Physics, Ryerson University, Toronto, Canada, for their help in experimental set up and data acquisition.

This work was partially supported by the Natural Sciences and Engineering Research Council of Canada (NSERC) Discovery Grant that was awarded to Prof. J. Tavakkoli.

REFERENCES

- Lafon C, Bouchoux G, Souchon R, Chapelon J. Monitoring and follow up of HIFU lesions by ultrasound. 4th IEEE International Symposium on Biomedical Imaging: From Nano to Macro, 2007. p. 1068-71.
- Clement GT. Perspectives in clinical uses of high-intensity focused ultrasound. *Ultrasonics* 2004;42:1087-93.
- Tavakkoli J, Sanghvi NT. Ultrasound-guided HIFU and Thermal Ablation. In: Frenkel V, editor. *Therapeutic Ultrasound: Mechanisms to Applications*. Hauppauge, NY: Nova Science Publishers; 2011. p. 137-61.
- Christakis D, Pavlou M, Velev O, Kyriakou K, Trimikliniotis M. High intensity focused ultrasound ablation of kidney guided by MRI. *Ultrasound Med Biol* 2004;30:397-404.
- Hynynen K. MRIGHIFU: A tool for image-guided therapeutics. *J Magn Reson Imaging* 2011;34:482-93.
- Khokhlova TD, Canney MS, Lee D, Marro Ki, Crum LA, Khokhlova VA, et al. Magnetic resonance imaging of boiling induced by high intensity focused ultrasound. *J Acoust Soc Am* 2009;125:2420-31.
- Vaezy S, Andrew M, Kaczkowski P, Crum L. Image-guided acoustic therapy. *Annu Rev Biomed Eng* 2001;3:375-90.
- Bailey MR, Khokhlova VA, Sapozhnikov OA, Kargl SG, Crum LA. Physical Mechanisms of the Therapeutic Effect of Ultrasound (A Review). *Acoust Phys* 2003;49:369-88.
- Ter Haar G. Therapeutic applications of ultrasound. *Prog Biophy Mol Biol* 2007;93:111-29.
- Seip R, Tavakkoli J, Wunderlich A, Narendra TS, Dines K, Crum L. Real-time detection of multiple lesions during High Intensity Focused Ultrasound (HIFU) Treatments. Seattle: International symposium on therapeutic ultrasound; 2002.
- Zhong H, Wan MX, Jiang YF, Wang SP. Monitoring imaging of lesions induced by high intensity focused ultrasound based on differential ultrasonic attenuation and integrated backscatter estimation. *Ultrasound Med Biol* 2007;33:82-94.
- Zhang S, Wan M, Zhong H, Xu C, Liao Z, Liu H, et al. Dynamic changes of integrated backscatter, attenuation coefficient and bubble activities during High intensity focused ultrasound (HIFU) treatment. *Ultrasound Med Biol* 2009;35:1828-44.
- Dalong L, Ebbini E. Real-time 2D Imaging of Thermal and Mechanical Tissue Response to Focused Ultrasound. 9th international symposium on therapeutic Ultrasound?ISTU 2009, AIP Conf Proc 2010; 1215:57-61.
- Zhang M, Castaneda B, Christensen J, Saad WE, Bylund K, Hoyt K, et al. Real-time sonoelastography of hepatic thermal lesions in a swine model. *Med Phys* 2008;35:4132-41.
- Hawa C, Arora M, Coussios C, Noble A. The Effect of Attenuation Coefficient on Radiation Force Impulse Monitoring of Thermal Lesions. 9th International Symposium On Therapeutic Ultrasound-ISTU 2010;1215:66-73.
- Anand A, Petruzzello J, Zhou S, Sethuraman S, Azevedo J. Two-Dimensional Real-time Ultrasound Technique to Control Lesion Size during HIFU Therapy. 9th International Symposium On Therapeutic Ultrasound-ISTU 2010;1215:79-82.
- Hou G, Lou J, Marquet F, Vappou J, Konofaqou E. Performance assessment of HIFU lesion detection by harmonic motion imaging for focused ultrasound (HMIFU): A 3-D finite-element-based framework with experimental validation. *Ultrasound Med Biol* 2011;37:2013-27.
- Meng-Lin L, Dai-Wei L, Hao-Li L, Ming-Shi L. Ultrasonic Nakagami visualization of HIFU-induced thermal lesions. *Ultrasonics symposium (IUS) IEEE, San Diego, California*; 2010. p. 2251-3.
- James SP, William DR. Segmenting ultrasound images of the prostate using neural networks. *Ultrasonic imaging. Ultrason Imaging* 1992;14:159-85.
- Dokur Z, Olmez T. Segmentation of ultrasound images by using a hybrid neural network. *Pattern Recognit Lett* 2002;23:1825-36.
- Kurnaz MN, Dokur Z, Olmez T. Segmentation of ultrasound images by using an incremental self-organized map. *Proceedings of the 23rd Annual EMBS International Conference* 2001;3:2638-40.
- Yousef AI, Samarasinghe S. Ultrasound based computer aided diagnosis of breast cancer: Evaluation of new feature of mass central.

- 19th International Congress On Modelling And Simulation, 2011. p. 1063-9.
23. Kuo S, Hsiao Y, Chen DR. Classification of benign and malignant breast tumors using neural networks and three-dimensional power doppler ultrasound. *Ultrasound Obstet Gynecol* 2008;32:97-102.
 24. Ophir J, Shawker TH, Maklad NF, Miller JG, Flax SW, Narayana PA, et al. Attenuation estimation in reflection: Progress and prospects. *Ultrasound Imaging* 1984;5:349-95.
 25. Rahimian S, Tavakkoli J. An acoustic backscatter-based method for estimating attenuation towards monitoring lesion formation in high intensity focused ultrasound. Theses and Dissertations 2012; paper 620 Available from: <http://www.digitalcommons.ryerson.ca/dissertations/620> [Last accessed on 2012].
 26. Shung KK. *Diagnostic Ultrasound: Imaging and blood flow measurement*. Kindle ed. Boca Raton FL: CRC Press, Taylor and Francis Group; 2006.
 27. Waters K, Cohen-Bacrie C, Levrier C, Fornes P, Pergrale J, Laugier P, et al. *In vitro* characterization of carotid plaque using a clinical ultrasound imaging system. *Ultrason Symp* 2001;2:1197-200.
 28. Chen J, Zagzebski J. Frequency dependence of backscatter coefficient versus scatterer volume fraction. *Ultrasonics, Ferroelectrics and Frequency Control*, IEEE Transaction on, 1996;43:345-53.
 29. Chen J, Zagzebski J. Frequency dependence of backscatter coefficient versus scatterer volume fraction. *IEEE Trans Ultrason Ferroelectr Freq Control* 1996;43:345-53.
 30. Kanzler S, Oelze M. Improved scatterer size estimation using backscatter coefficient measurements with coded excitation and pulse compression. *J Acoust Soc Am* 2008;123:4599-607.
 31. Davignon F, Deprez JF, Basset OA. Parametric imaging approach for the segmentation of ultrasound data. *Ultrasonics* 2005;43:789-801.
 32. Tsui P, Chang C. Imaging local scatterer concentrations by the Nakagami statistical model. *Ultrasound Med Biol* 2007;33:608-19.
 33. Ho MC, Lin JJ, Shu YC, Chen CN, Chanq CC, Tsui PH. Using ultrasound Nakagami imaging to assess liver fibrosis in rats. *Ultrasonics* 2012;52:215-22.
 34. Tsui P, Liao Y, Chanq CC, Kou WH, Chanq KJ, Yeh CK. Classification of benign and malignant breast tumors by 2-D analysis based on contour description and scatterer characterization. *IEEE Trans Med Imaging* 2010;29:513-22.
 35. Destempes F, Cloutier GA. critical review and uniformized representation of statistical distributions modeling the ultrasound echo envelope. *Ultrasound Med Biol* 2010;36:1037-51.
 36. Kanai H. Propagation of spontaneously actuated pulsive vibration in human heart wall and *in vivo* viscoelasticity estimation. *IEEE Trans Ultrason Ferroelectr Freq Control* 2005;52:1931-42.
 37. Song J, Venkatesh S, Conant E, Cary T, Arger P, Sehgal C. Artificial neural network to aid differentiation of malignant and benign breast masses by ultrasound imaging. *Med Imaging* 2005;5750: 148-52.

How to cite this article: Rangraz P, Behnam H, Shakhssalim N, Tavakkoli J. A feed-forward neural network algorithm to detect thermal lesions induced by high intensity focused ultrasound in tissue. *J Med Sign Sens* 2012;2:192-202.

Source of Support: Natural Sciences and Engineering Research Council of Canada (NSERC) Discovery Grant, **Conflict of Interest:** None declared

BIOGRAPHIES



Parisa Rangraz received the B.Sc. degree in 2004, the M.Sc. degree in 2007 and the Ph.D. degree in 2012, all in biomedical engineering from the Science and Research Branch, Islamic Azad University. Her research interests include Ultrasound in Medicine, Medical signal processing, Ultrasound guided HIFU.

E-mail: p.rangraz@srbiau.ac.ir



Hamid Behnam received the B.S. degree in Electrical Engineering from Iran University of Science and Technology, Tehran, Iran, in 1988, the M.S. degree in Medical Engineering from Sharif University of Technology, Tehran, Iran, in 1992, the Ph.D. degree in Applied Electronics from Tokyo Institute of Technology, Tokyo, Japan in 1998. Since 1998 till 2004, he was a researcher at Iran Research Organization for Science and Technology and from 2004 he has been a faculty member at Iran University of Science and Technology, in Tehran, Iran. Currently he is an Assistant Professor of Biomedical Engineering at the IUST. His research interests are Ultrasound in Medicine, Medical Image processing and Medical signal processing.

E-mail: behnam@iust.ac.ir



Nasser Shakhssalim received M.D. from Mashhad University of Medical Sciences in 1996; he was Urology Resident during 1999-2003 and Urology Chief Resident during 2003-2004 in Shahid Beheshti University of Medical Sciences-Shahid Labbafinejad Medical Center and he received National board certification in Urology (Iran) in 2004. He has been a faculty member of Shahid Beheshti University of Medical Sciences, Urology/Nephrology Research Center (UNRC), Deputy for Research in UNRC and Clinical practice in Shahid Labbafinejad Medical Center since 2006.

E-mail: slim456@yahoo.com



Jahan Tavakkoli obtained a BSc degree in Electrical Engineering and a MSc degree in Biomedical Engineering, both from Sharif University of Tech., Tehran, Iran. He obtained a PhD degree with the highest honors in Biomedical Physics from University of Lyon-1, and research laboratory of INSERM, Unit 556, Lyon, France, in 1997. He also completed a post-doctoral fellowship in Biomedical Engineering at University of Toronto, Toronto, Canada, in 1998. He has over 20 years of professional experience in both academia and industry in biomedical applications of ultrasound in therapy and imaging, and in ultrasound modeling and simulation. He has been holding R&D positions in several leading high-tech medical device companies including: Focus Surgery Inc., Indianapolis, IN; Visualsonics Inc., Toronto, Canada; and Guided Therapy Systems LLC, Mesa, AZ. He is currently an Assistant Professor in Dept. of Physics, Ryerson University, Toronto, Canada, and an Affiliate Scientist in Keenan Research Center, St. Michael's Hospital, Toronto, Canada. Most of Dr. Tavakkoli's research and development projects have been funded by grants from federal and provincial funding agencies, and by medical devices industry (NIH, NSERC, ORF-RE, etc.). He is the co-founder and co-director of "Advanced Biomedical Ultrasound Imaging and Therapy Laboratory" in the Dept. of Physics of Ryerson University. Dr. Tavakkoli is an active member of several professional scientific societies including: IEEE Ultrasonics, Ferroelectrics, and Frequency Control; IEEE Engineering in Medicine and Biology; Acoustical Society of America; Canadian Acoustical Association; International Society for Therapeutic Ultrasound; and Ultrasonic Industry Association. Among other positions, he is the Associate Editor, Journal of Medical Physics; the Associate Editor, Bio-acoustics, Journal of Canadian Acoustics; and the Member of Technical Committee, Biomedical Ultrasound/Bioresponse to Vibrations, Acoustical Society of America. He has published over 80 scientific papers in peer-reviewed journals and international conferences in the areas of biomedical ultrasound therapy and imaging.

E-mail: jtavakkoli@ryerson.ca